Pergamon

PII: S0038–092X(00)00042–6

Solar Energy Vol. 67, Nos. 1–3, pp. 93–100, 1999

0038-092X/99/$ - see front matter

www.elsevier.com/locate/solener

A CFD HEAT TRANSFER ANALYSIS OF THE TRANSPIRED SOLAR COLLECTOR UNDER NO-WIND CONDITIONS

S. J. ARULANANDAM*, K. G. TERRY HOLLANDS**,† and E. BRUNDRETT**
*Department of Mechanical Engineering, University of Alberta, Edmonton, AB, Canada
**Department of Mechanical Engineering, University of Waterloo, Waterloo, ON, Canada

Received 16 September 1999; revised version accepted 4 February 2000

Communicated by VOLKER WITTWER

Abstract—The unglazed transpired solar collector is now a well-recognised solar air heater for heating outside air directly. Example applications include pre-heating ventilation air and heating air for crop drying. The outside air in question is sucked straight from ambient, uniformly through the whole surface of a perforated blackened plate (the absorber plate) exposed to the sun. An important parameter fixing the collector's efficiency is the heat exchange effectiveness, ε. Once ε is known, finding the collector efficiency is straightforward. The effectiveness depends on the wind speed, the suction velocity, and the plate geometry. This paper is about determining this effectiveness by computational fluid mechanics (CFD), for conditions of no wind. Because of symmetry, the computational domain needed only to extend over a representative element, which included one hole and the region immediately adjacent to it extending to half the distance between holes. Simulations were carried out over a wide range of conditions, and the results are incorporated into a correlation model. Because of the no-wind assumptions, the model is of limited direct use, but when combined with experimental data, the model can permit a wider-ranging correlation equation to be obtained.

1. INTRODUCTION

Unglazed transpired-plate solar air-heating collectors have been the subject of a number of recent investigations. They are effective devices for cases where outside air is to be heated directly, such as in heating ventilation air for buildings and for drying applications. The outside air in question is drawn straight from ambient, through the entire surface of a perforated blackened plate. The glazing, traditionally used for reducing the plate's radiant and convective losses, is dispensed with in this collector. It is not required, because the convective boundary layer is continually sucked off, thus virtually eliminating the convective loss. In addition, the intimate heat transfer between the plate and the sucked air keeps the plate temperature low, minimizing the radiant loss. In commercial production, these collectors have been built to cover areas on the sides of buildings of the order of thousands of square metres.

The available heat transfer theory (Kutscher *et al*., 1993; Hollands, 1998) allows one to predict the collector efficiency, but only once a quantity called the heat exchange effectiveness, ε, has been specified. Defined as the actual temperature rise of the air as it passes through the plate divided by the maximum possible temperature rise, ε is a measure of the intimacy of the convective heat transfer between the plate and the air, and can be determined by purely convective considerations and/or analyses. Most published studies have determined ε experimentally (Kutscher, 1994; Van Decker *et al*., 1996, 1999).

This paper is about determining this effectiveness by computational fluid mechanics (CFD). CFD studies of the problem have been carried out before. Thus Kutscher (1992) carried out CFD studies on a plate with circular holes, but the range of parametric settings did not extend over the full range of interest, because of the limitations of the code and computational capability. The CFD studies of Cao *et al.* (1993) covered a wide range of parameters, but it was restricted to long slit-like perforations rather than the more common circular holes. Because of the limitations of CFD simulations in the present study, it was necessary to place important restrictions on the problem statement: the assumption of no-wind conditions and the exclusion of the effect of the heat transfer on the back of the plate. But given these conditions, the simulations were carried out

†Author to whom correspondence should be addressed. Tel.: +1-519-888-4053; fax: +1-519-888-6197; e-mail: kholland@solar1.uwaterloo.ca

over a wide range of parametric settings, and the results are incorporated into a correlation model. Because of the assumptions, the model is of limited direct use, but when combined with experimental data, it has permitted a wide-ranging correlation equation to be obtained (Van Decker *et al*., 1996; Van Decker and Hollands, 1999).

2. MODEL DEVELOPMENT

2.1. Defining the domain

Fig. 1a is a sketch of the transpired plate with circular holes on a square pitch arrangement in zero wind. The spacing between the holes centres is the hole pitch *P*. Since every hole should behave in a similar manner, one need only study a representative element, like the one shown in a dotted line in Fig. 1a. Several planes of symmetry, introduced by the fact that there is no wind, imply that one need only study the reduced domain sketched in Fig. 1b with symmetry boundary conditions applying at the planes $z = 0$, $z = P/2$, $y = 0$, and $y = P/2$. The computational domain is also bounded by the planes $x = 0$ and $x = x_\infty$. In the drawing, V_s represents the suction velocity, or the volumetric rate at which air is sucked through the plate per unit plate area. At distance x_∞ from the plate this air stream is assumed to be in uniform motion.

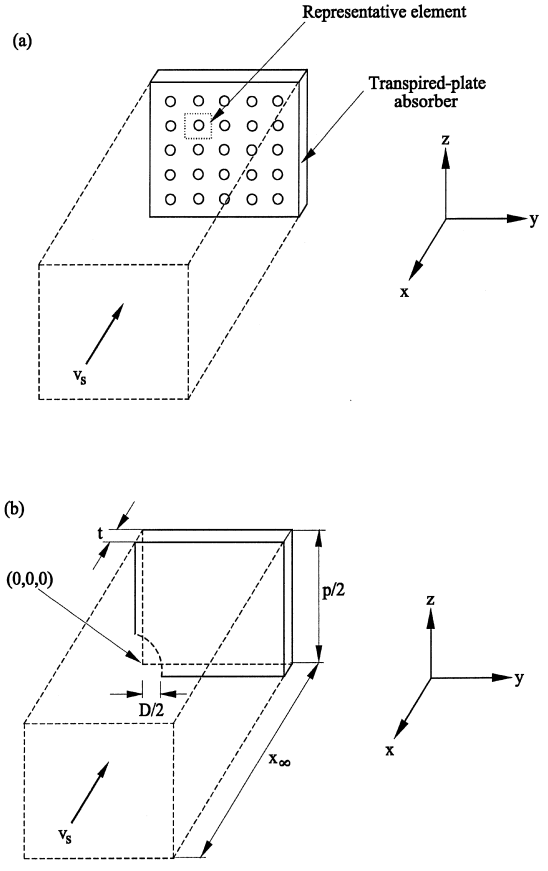

Fig. 1. (a) Sketch of the representative elements of the absorber plate and (b) definition of the computational domain.

2.2. Governing equations and boundary conditions

The relevant governing equations for the air velocity $\vec{V} = (u, v, w)$ and the temperature T are the equations for the conservation of mass, momentum, and energy, assuming laminar flow, steady conditions, constant properties, no external forces and no viscous heat dissipation. These are given in textbooks (e.g. Arpaci and Larsen, 1984) and will not be repeated here. For the region containing the solid (i.e. the plate), the governing equation is simply the steady heat diffusion equation.

The inlet boundary condition is the plane $x = x_\infty$. Ideally, this plane would be located an infinite distance from the plate, but any CFD representation has to place it at a finite distance of magnitude sufficiently large to realistically represent the infinite distance. The following boundary conditions were assumed to apply there:

$$\text{at } x = x_\infty,\ \vec{V} = (V_s, 0, 0), \quad T = T_\infty, \quad P = P_\infty \qquad (1)$$

where T_∞ and P_∞ are the ambient air temperature and pressure, respectively. We modelled the back of the plate as adiabatic, so that

$$\text{at } x = 0 \text{ and for } y^2 + z^2 \geq D^2/4, \quad \frac{\partial T}{\partial x} = 0. \qquad (2)$$

The other part of the $x = 0$ plane is the flow outlet plane, which was given the outflow boundary condition (Patankar, 1980):

$$\text{at } x = 0 \text{ and for } y^2 + z^2 \leq D^2/4, \quad \frac{\partial T}{\partial x} = 0,$$
$$u \geq 0. \qquad (3)$$

The boundary conditions along the planes of symmetry are as follows:

$$\text{at } y = 0 \text{ or } y = P/2, \frac{\partial u}{\partial y} = 0, v = w = 0,$$
$$\frac{\partial T}{\partial y} = 0, \quad u \geq 0 \qquad (4)$$

$$\text{at } z = 0 \text{ or } z = P/2, \frac{\partial u}{\partial z} = 0, v = w = 0,$$
$$\frac{\partial T}{\partial z} = 0, \quad u \geq 0. \qquad (5)$$

For the front surface of the plate, we have

at $x = t$ and $y^2 + z^2 \geq D^2/4$, $\vec{V} = (0, 0, 0)$,

$$\alpha G = -k_s \left.\frac{\partial T}{\partial x}\right|_{t-} - k \left.\frac{\partial T}{\partial x}\right|_{t+} + h_r(T - T_\infty) \tag{6a}$$

where G is the solar irradiance, α is the solar absorptivity of the plate, k_s and k are the thermal conductivity of the plate and air, respectively, and h_r is the radiative heat transfer from the plate to the radiant surrounds, which are assumed to be at the ambient air temperature, T_∞. At the interface inside the hole, there must be a balance of heat fluxes, leading to the boundary condition:

at $0 \leq x \leq t$ and for $y^2 + z^2 \geq D^2/4$,

$$\vec{V} = (0, 0, 0), \; -k \left.\frac{\partial T}{\partial r}\right|_{(D/2)^-} = -k_s \left.\frac{\partial T}{\partial r}\right|_{(D/2)^+} \tag{6b}$$

where $r^2 = y^2 + z^2$, r being the radial co-ordinate in the corresponding cylindrical co-ordinate system.

2.3. Dimensional analysis

The governing equations and boundary conditions were transformed into non-dimensional equations by introducing certain dimensionless variables (Arulanandam *et al*., 1995). The following dimensionless groups arose: the plate porosity $\sigma = \pi D^2/4P^2$, a Reynolds number defined by

$$Re_D = V_h D/\nu \text{ where } V_h = V_s/\sigma \tag{7}$$

a non-dimensional approach distance $x_\infty^* = x_\infty/D$, and a non-dimensional plate thickness $t^* = t/D$, the 'plate admittance' *Ad*, and radiative Nusselt number Nu_r defined by

$$Ad = k_s t/kD \text{ and } Nu_r = h_r D/k, \tag{8}$$

respectively, and the Prandtl number of air, which is fixed at about 0.7. The heat exchange effectiveness ε is defined by $(T_0 - T_\infty)/(T_p - T_\infty)$ where T_0 is the bulk outlet air temperature at $x = 0$ and T_p is the average plate temperature. When ε is expressed in terms of dimensionless quantities, there results

$$\varepsilon = \varepsilon(Re_D, \sigma, t^*, Ad, Nu_r). \tag{9}$$

The heat transfer can also be expressed in terms of a Nusselt number, defined by

$$Nu = -Re_D \, Pr \, \sigma \ln(1 - \varepsilon). \tag{10}$$

From Eqs. (9) and (10) it follows that

$$Nu = Nu(Re_D, \sigma, t^*, Ad, Nu_r). \tag{11}$$

3. COMPUTATIONAL FLUID MECHANICS MODEL

The governing equations were solved with the appropriate boundary conditions using TASCflow (Anon, 1994), a finite volume-based CFD code. Using TASCflow, the computational domain shown in Fig. 1b was divided into a finite set of control volumes. The TASCflow solver was used to solve the algebraic equations that result from integrating the governing equations over each control volume. The control volume formulation method is fully conservative, with the formulation guaranteeing conservation of mass, momentum, and energy over each control volume.

3.1. Grid design

The domain was broken down into a set of control volumes, with a node at the centre of each volume. The total number of nodes N in the resulting grid is limited by constraints on the available computer memory and also by CPU time.

In breaking down the domain, a rectilinear grid with uniformly spaced nodes was tried, but there were several problems with this approach, the most significant being the large number of irregular control volumes located at the edge of the circular hole. Later a series of straight lines approximating circular arcs centred along the x-axis was used to create the grid in the region within $D/2$ of the centreline. A different series of straight lines was used to approximate the square cross-section of the domain at the edges of the domain. This choice of grid lines improved the grid in the vicinity of the hole, but it led to having several nodes co-located at the origin. So an additional grid was created for the region around the x-axis, and this was then attached to the main grid. Thus, the final grid actually consisted of two grids: the main grid and the sub-grid. A view of the final grid design is given in Fig. 2.

Preliminary investigations indicated that convergence was improved by increasing the number of nodes near the solid and inside the hole in order to fully capture the characteristics of the flow as it approaches the plate and enters the hole. Therefore, the nodes were distributed using an expansion ratio R, where R is the ratio (in a given direction) of the length of the last flux element to that of the first flux element. The expansion ratio used in the grid construction near the walls was 25, resulting in a higher density of grid points in regions near the walls, where they were most needed.

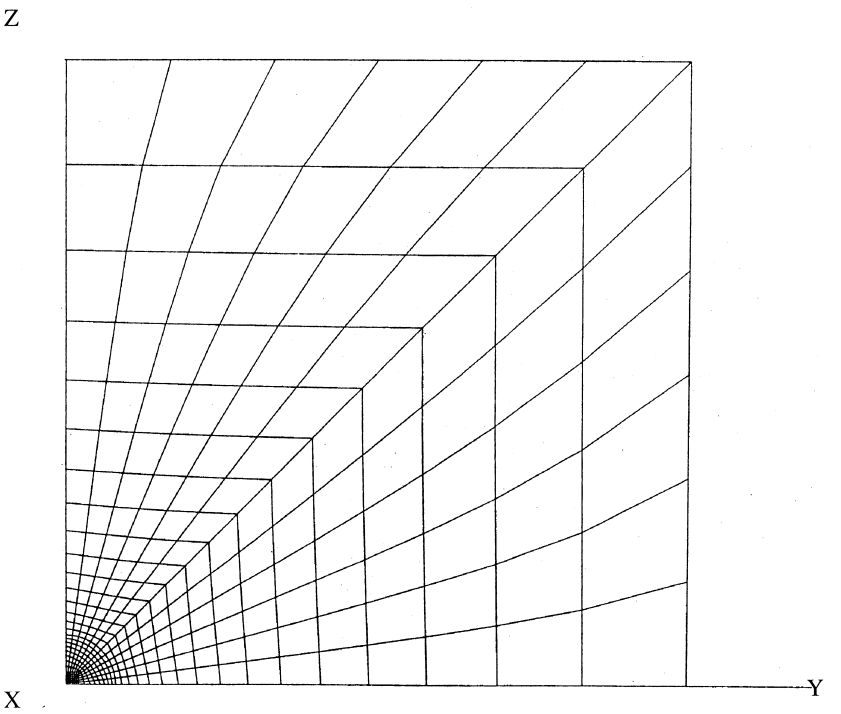

Fig. 2. Plot of the grid lines used at a constant x-plane.

3.2. Grid refinement and other preliminary studies

The approximations introduced in the discretization process become more precise as the gird is refined, i.e. as the number of nodal points N is increased. Grid refinement studies are used to study the sensitivity of the numerical solution to the size of the grid and then decide what value of N will be used for the bulk of the simulations. A grid refinement study is usually carried out by systematically increasing the number of nodes and comparing the results — in terms of global parameters, such as the effectiveness. For a three-dimensional problem, the number of flux elements is successively doubled in all of the three directions. Thus, if the first grid has N_1 nodes in total, the second will have $8N_1$ and the third $64N_1$ and so on. The solution as N approaches infinity can be extrapolated from the finite N grid solutions by using an extrapolation method such as Repeated Richardson (RR) extrapolation (Zwillinger, 1992). Comparing the global parameters from each finite grid with the extrapolated results can then be used to estimate the error induced by having a finite value of N.

In the present study, the grid refinement study was completed using the following combination of parameters: $Re_D = 1375.5$, $\sigma = 0.0005$, $t^* = 0.67$, $Ad = 4.93$, and $Nu_r = 0.26$. This combination of parameters, having a high suction velocity, low conductivity and low porosity was the most difficult computationally, because it has high velocity gradients inside the hole and a large variation in temperature across the plate.

Ideally the x_∞^* plane is located an infinite distance in front of the plate, but in practice a suitably large value must be used. Several runs were made in which x_∞^* was reduced in steps of about 10 from 168 to 42. Within round-off error, the same results were obtained at each setting. So, at $x_\infty^* = 42$, the inlet boundary face is far enough away from the plate to not affect the results. Thus, a value of $x_\infty^* \geq 42$ was used for the grid refinement study and all subsequent simulation runs.

An initial coarse grid, Grid A, was first constructed using a $6 \times 12 \times 12$ grid with six flux elements in the x-direction, 12 flux elements in the y-direction, and 12 flux elements in the z-direction. (A flux element is a hexahedron defined by eight nodes, one at each vertex.) The number of flux elements in Grid A was doubled in the three directions to produce Grid B, a $12 \times 12 \times 24$ grid. Similarly, Grid B was doubled to produce Grid D, a $24 \times 48 \times 48$ grid. Computer memory limitations eliminated the possibility of running a fourth grid by doubling Grid D. Instead, a fourth grid, between Grid B and Grid D, was constructed by using a refinement factor of 1.5; thus Grid C was an $18 \times 36 \times 36$ grid. The effectiveness was calculated for the four different grids and plotted

Table 1. Grid refinement study results: $Re_D = 1375.5$, $\sigma = 0.005$, $t^* = 0.67$, $Ad = 4.93$, $Nu_r = 0.26$

Grid size	Global parameters	
	ε	η
Grid A (6×12×12)	0.1745	81.98%
Grid B (12×24×24)	0.1473	66.78%
Grid C (18×36×36)	0.1365	66.60%
Grid D (25×48×48)	0.1362	66.45%
RR extrapolation	0.1362	66.45%

against the inverse of N. The Repeated Richardson (RR) extrapolation method was used to estimate the value of the effectiveness and the efficiency as the number of nodes approached infinity, and the results are presented in Table 1.

Based on the results of this study, and considering the amount of CPU time available, Grid C was chosen as a suitable grid with acceptably small error and convergence time. Fig. 3 gives a plot of the velocity vectors obtained using Grid C.

3.3. Dimensionless parameter validation study

A study was undertaken with two different sets (set 1 and set 2) of dimensional variables chosen such that the dimensionless parameters were the same (namely $Re_D = 540$, $\sigma = 0.0111$, $t^* = 2.0$, $Ad = 1150$, and $Nu_r = 0.35$) but the dimensional parameters were different, as follows: $D_1 = 0.001588$ m, $P_1 = 0.0134$ m, $t_1 = 0.003175$ m, $V_{s1} = 0.06$ m/s, $k_{s1} = 15.12$ W/mK, $\varepsilon_{p1} = 0.45$; and $D_2 = 0.001191$ m, $P_2 = 0.01$ m, $t_2 = 0.002382$ m, $V_{s2} = 0.08$ m/s, $k_{s2} = 15.12$ W/mK, $\varepsilon_{p2} = 0.60$. (In the proceeding, subscripts 1 and 2 refer to the two sets, and ε_p is the emissivity of the plate.) The resulting values for ε were $\varepsilon_1 = 0.367$ and $\varepsilon_2 = 0.366$, which are within 0.3% of each other, verifying the integrity of the computational code and demonstrating that the behaviour of ε is indeed captured by the variables in Eq. (9).

3.4. Comparison to similar studies

Kutscher (1992) completed numerical studies for a transpired plate absorber with a hexagonal pitch under no-wind conditions. While not identical to the square-pitch configuration investigated in the current study, the configurations were similar enough to merit a detailed comparison of the results. Kutscher's work covered high porosity isothermal plates and include heat transfer from the back of the plate, but in the current numerical model the back surface of the plate has been modelled as an adiabatic surface. This significant

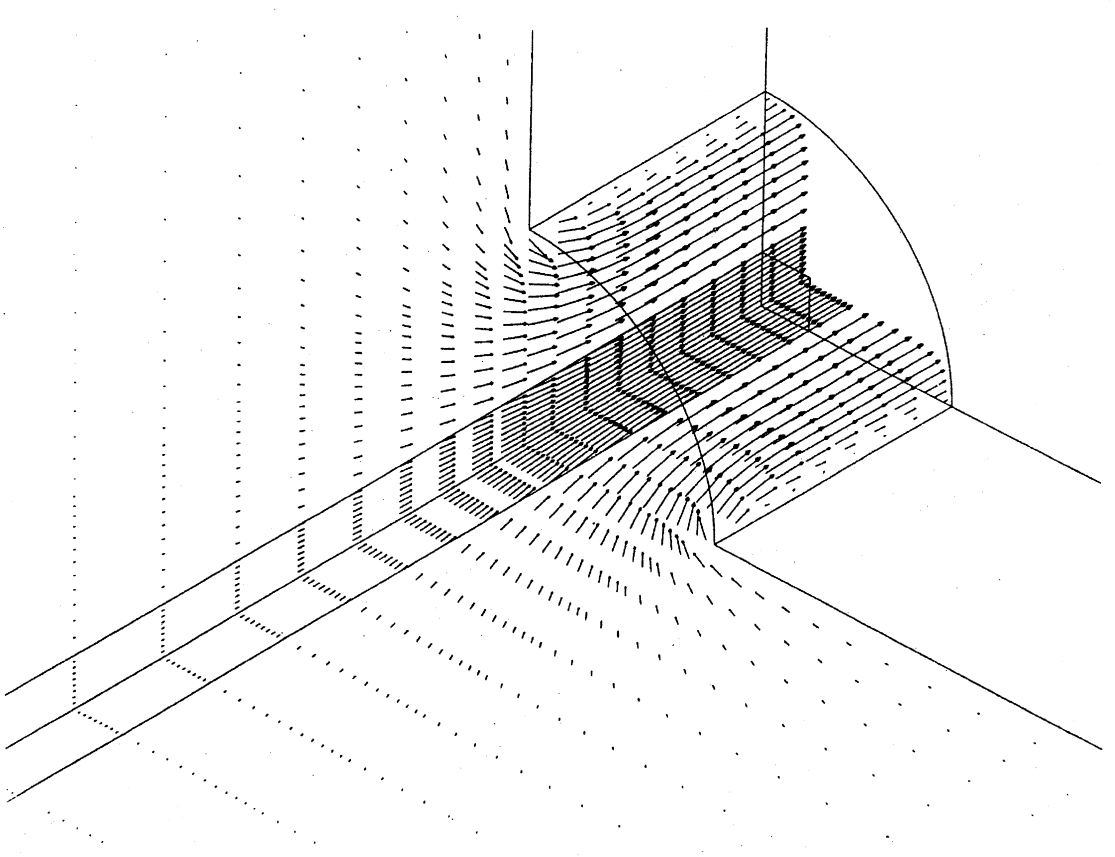

Fig. 3. Fluid velocity vector plot obtained in the set of conditions applying in Grid C of the grid refinement study.

difference in the models was easily accounted for in the comparison of Kutscher's numerical results, since he broke down the total heat transfer into three sequential heat exchange processes: that occurring along the front surface of the plate, inside the hole, and along the back surface of the plate. To compare the present results, Kutscher's results for the front and hole regions were combined. The results of the two codes were found to agree to within about 1%. Further details are given by Arulanandam (1995).

4. SIMULATION RESULTS

4.1. Range of parameters

The important ranges for the non-dimensional parameters were chosen based on a number of factors, including manufacturing constraints and solver limitations. Thus, the following ranges were specified for the dimensionless parameters: $150 \leq Re_D \leq 1350$, $0.005 \leq \sigma \leq 0.02$, $0.67 \leq t^* \leq 2.0$, $5 \leq Ad \leq 1150$, and $0.13 \leq Nu_r \leq 0.52$. The physical properties of air were kept constant for all simulations, evaluated at 300 K and atmospheric pressure. The ambient air temperature, T_∞, is 300 K. A constant value of $\alpha G = 800$ W/m^2 is used for all simulations. Simulations were carried out over a wide range of combinations of specific values of the dimensional parameters inside their ranges: a total of 216 simulations were carried out in all.

4.2. Simulation results

To illustrate the effect of the five dimensionless parameters on the collector performance, plots were prepared in which each parameter was varied while the others were held constant. Fig. 4 shows a typical plot of this set. The strongest effect on ε was observed for Re_D; the next strongest was observed for σ, then t^*, and then *Ad*. No effect of Nu_r was observed. Further plots are given by Arulanandam (1995).

Fig. 4 demonstrates the effect of the admittance. The admittance, *Ad*, represents the ability of the plate to conduct heat. Because of the high conductive coefficient near the hole associated with the high velocities there, the region of the plate surrounding the hole takes up a lower temperature than the rest of the plate. Heat from the outer regions of the plate is therefore conducted towards the hole. For high *Ad* plates, more heat is conducted towards the hole, increasing ε. In the high *Ad* cases, corresponding for example to plates made of stainless steel ($k_s = 15.121$ W/m K) or aluminium ($k_s = 131$ W/m K), the value of ε approaches the asymptotic value; the asymptote is approached as the plate approaches isothermal conditions with the plate temperature almost uniform. At low values of *Ad*, the non-uniform temperature distribution results in higher temperatures away from the hole, leading to higher radiative losses in this region and thus lowering ε.

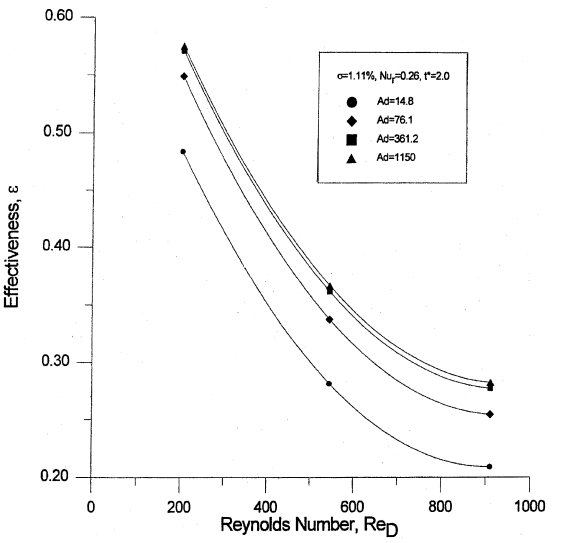

Fig. 4. Plot of simulation results in the form of effectiveness vs. Reynolds number at various values of the admittance Ad. Values of σ, Nu_r, and t^* are as noted.

4.3. Development of correlation equation

One of the objectives in this study was to relate the collector performance parameter ε to the non-dimensional parameters Re_D, σ, t^*, *Ad*, and Nu_r. One way to express the dependence of ε on these parameters is through the Nusselt number. That is, from the analysis presented in Section 2, the heat exchange effectiveness ε can be expressed as a function of Nu_D (Eq. (10)), and then Nu_D can be correlated as a function of these five dimensionless parameters. Once $Nu_D(Re_D, \sigma, t^*, Ad, Nu_r)$ is known, ε can be easily found using equations presented in Section 2.3. This is the strategy adopted here.

The statistical software package SAS was used to perform a non-linear multi-variable regression analysis of the data points generated using TASCflow. The curve fit program minimises the sum of the squares of the differences between the correlation equation values and the data points.

That Nu_r does not have a significant effect was confirmed by the SAS results. As a result, the correlation equation was developed for only four parameters: Re_D, σ, t^*, and *Ad*.

A simple power law form was used to capture the effects of Re_D and σ on Nu_D. The form used to capture the other variables took into account the behaviour of Nu_D as t^* and Ad approached the limits of 0 and ∞. Several forms were tried, but the best results were obtained using the equation of the form:

$$Nu_D = \frac{\beta_0 Re_D^{\beta_1} \sigma^{\beta_2} (1 + \beta_3 t^*)}{1 + \dfrac{\beta_4}{\beta_5 + Ad}}. \quad (12)$$

Using SAS, the values of the coefficients were found, and the best-fit correlation followed. This fit had a coefficient of determination, R^2, of 0.9915. (In the following, the correlation data and the TASCflow generated data will be distinguished by subscripts: C being used for correlation data and T for TASCflow data.) Following this, to check the limits, additional runs were completed for plate conductivity approaching zero and infinity. The additional points were added to the original simulation study data points, resulting in the following equation:

$$Nu_D = \frac{5.25\, Re_D^{0.36} \sigma^{0.78} (1 + 0.15 t^*)}{1 + \dfrac{7.89}{13 + Ad}}. \quad (13)$$

Fig. 5 is a plot of all of the data points used to generate the coefficients in Eq. (13), with $Nu_{D,T}$ plotted against $Nu_{D,C}$ calculated with Eq. (13). The coefficient of determination for this fit is $R^2 = 0.9887$. Although this R^2 value is lower than that obtained without the additional points, the result is a better fit for the data limits of Ad, i.e. as Ad approaches zero and as Ad approaches infinity.

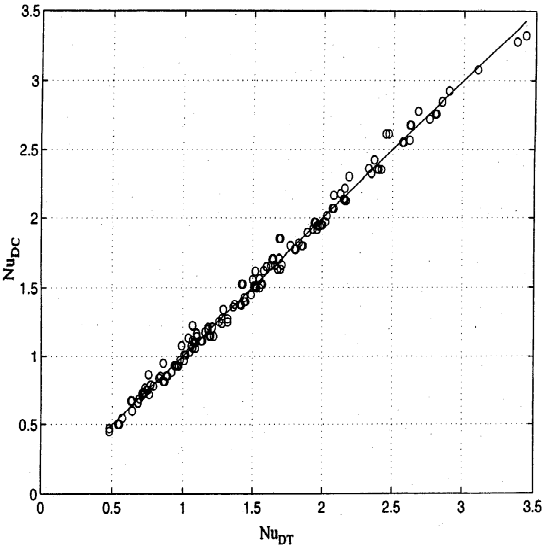

Fig. 5. Comparison of predictions of Nu_D given by Eq. (13) (denoted $Nu_{D,C}$) with the corresponding Nu_D given by the CFD simulation (denoted $Nu_{D,T}$).

Two additional forms of the correlation equation were tested in an attempt to improve the data fit. First, a higher order term in t^* was added to the numerator of the expression on the right-hand side of Eq. (13), then a higher order term in Ad was added to the denominator. The improvement with the additional terms was negligible in both cases. Thus, Eq. (13) was chosen as the most suitable fit for the data.

5. CONCLUSIONS

The heat transfer and flow characteristics have been investigated for a representative element of an unglazed transpired-plate absorber with holes in a square pitch arrangement under no-wind conditions. The study was completed using TASCflow, a state-of-the-art CFD code. A mathematical model was developed with the relevant boundary conditions and interfacial (solid–fluid) conditions specified. A dimensional analysis of these equations established that ε depends on five non-dimensional parameters: Re_D, σ, t^*, and Ad using Eq. (13). The computational grid was designed to handle a wide range of the dependent parameters for the simulation study. Validation of this grid was established by completing a multi-step grid refinement study, a dimensionless parameter dependence study, and a comparison with published data from Kutscher (1992). The simulation study was conducted by systematically varying each of the five dimensionless parameters for a total of 216 runs and analysing the results. Using SAS, a statistical software package, a correlation equation was derived for Nu_D ($R^2 =$ 0.9887). The Nusselt number is shown to be almost independent of Nu_r and can be estimated as a function of Re_D, σ, t^*, and Ad using Eq. (13).

The results demonstrate the potential for low conductivity absorbers in low porosity, low flow situations. For the same plate geometry, changing the plate conductivity from $k_s = 0.196$ W/m K to $k_s = 15.121$ W/m K resulted in a 10–20% drop in the effectiveness, with the percent reduction increasing as Re_D was increased. The effect on the thermal efficiency, η, would be less pronounced, with approximately a 5% reduction in η expected. The results of this study demonstrate that if transpired-plate absorbers were to be made from lower conductivity materials, such as plastics, acceptable efficiencies could still be achieved.

REFERENCES

Anon (1994). *TASCflow-Version 2.3.1: Theory Documentation*, Advanced Scientific Computing, AEA Technology Engineering Software, Waterloo, Canada.

Arpaci V. S. and Larsen P. S. (1984). *Convection Heat Transfer*, Prentice-Hall, New Jersey.

Cao S., Hollands K. G. T. and Brundrett E. (1993) Heat exchange effectiveness of unglazed transpired-plate solar collector in 2D flow. In Proceedings of ISES Solar World Congress 1993, Budapest, Hungary, Vol. 5, p. 351.

Hollands K. G. T. (1998) Principles of the transpired-plate air heating collector: the SOLARWALL. In *Renewable Energy Technologies in Cold Climates, 1998 Annual Meeting of the Solar Energy Society of Canada Inc*, p. 139, SESCI, Ottawa.

Kutscher C. F. (1992). *An Investigation of Heat Transfer for Air Flow through Low Porosity Perforated Plates*, University of Colorado, Department of Mechanical Engineering, Ph.D. Thesis.

Kutscher C. F. (1994) Heat exchanger effectiveness and pressure drop for air flow through perforated plates, with and without crosswind. *J. Heat Transfer* **116**, 391.

Kutscher C. F., Christensen C. and Barker G. (1993) Unglazed transpired solar collectors: heat loss theory. *ASME J. Solar Eng.* **115**(3), 182.

Van Decker G. W. E., Hollands K. G. T. and Brunger A. P. (1996) Heat exchange effectiveness of unglazed transpired-plate solar collector in 3D flow. In *Proceedings of EuroSun '96, Freiburg, Germany*, Goetzburger A. and Luther J. (Eds.), p. 130, DGS-Sonnen energie Verlags GmbH, Munchen, Germany.

Van Decker G. W. E. and Hollands K. G. T. (1999) An empirical heat transfer equation for the transpired solar collectors, including no-wind conditions. In *Proceedings, Solar World Congress, 1999: Biennial Meeting of the International Solar Energy Society, Jerusalem, Israel*, International Solar Energy Society, Freiburg, Germany.

Zwillinger D. (1992). *Handbook of Integration*, John Bartlett, Boston.